Journal of Engineering Mathematics 22: 15–42 (1988)
© Martinus Nijhoff Publishers, Dordrecht – Printed in the Netherlands

The turbulent boundary layer and wake of an aligned flat plate

A. NEISH and F.T. SMITH
Department of Mathematics, University College London, Gower Street, London WC1E 6BT, UK

Received 12 May 1987; accepted 21 September 1987

Abstract. A theoretical study of the turbulent boundary layer and symmetric wake of an aligned flat plate is described. A specific turbulence model is taken throughout, namely the Cebeci–Smith one, although at the high Reynolds numbers of interest the wake results are found subsequently to be influenced hardly at all by the precise details of the model, so that there is a ready generalization. The two-tiered wake implied by the analysis is rather different from the two-tiered boundary layer. The inner tier of the wake is thicker than the boundary layer's inner tier and, associated with this, the "logarithmic" zone present in the boundary layer upstream is absent in the wake, being replaced by a "cuspidal" zone just outside the inner-wake tier due to the reduction in shear stresses. Local interactive regions near the trailing edge show how the erosion of the logarithmic behaviour takes place relatively fast, being virtually complete on entry into the full wake. The agreement between the theory, experiments and previous computations for the boundary layer and full wake is found to be good quantitatively as well as qualitatively, encouraging the use of the present approach in other contexts such as turbulent separation.

1. Introduction

The turbulent flow past a flat plate aligned with a uniform free stream poses a fundamental problem theoretically, with particular concern over its properties at high Reynolds numbers. It is in addition of more practical interest since it can provide guidance for the prediction of the turbulent flow past thin airfoils and for increased understanding of the main flow features, including the change in character near the trailing edge and in the wake and, possibly, the onset of turbulent separation on thicker airfoils. Experimental studies of the turbulent flat-plate flow have been made by Chevray and Kovasznay [1] and Andreopoulos and Bradshaw [2] at Reynolds numbers of approximately 6.5×10^5 and 6.7×10^6, respectively, based on the plate length. Both studies present detailed measurements of the velocity profiles in the wake and the displacement and other thickness quantities there, with the second, more exhaustive, study being concentrated relatively nearer the trailing edge and giving also measurements of the velocity fluctuations and intensity distributions in the near wake. Comparisons with the above experiments are made later in this report, although alternative sets of experiments are presented by Pot [3] and Ramaprian, Patel and Sastry [4] and in references quoted in the above papers.

The largeness of the Reynolds number in practice is reflected in the corresponding computational and/or theoretical investigations. Notably, Mellor [5], Bush and Fendell [6] and Fendell [7] developed an asymptotic approach for the attached turbulent boundary-layer description assuming a rather general form for the turbulence closure consistent with a two-tiered boundary layer. This has been followed through, and extended significantly, by Melnik and his co-workers [8–11] for the examination of trailing-edge motions, interactive effects (see also Sykes [12]) and transonic conditions, while proposals for the structure of turbulent separation have been put forward by Sychev and Sychev [13] and Sychev [14] as

discussed later in this section. The flow near a trailing edge has also been considered by Alber [15] and more recently by Bogucz and Walker [16], the latter work being done simultaneously with ours and kindly brought to our attention by Prof. J.D.A. Walker. Comments on the small overlap of these papers and the present study are made in our Appendix B below. On the computational side the flat-plate flow, and others, have been addressed numerically by Cebeci, Thiele, Williams and Stewartson [17] using a set of classical boundary-layer equations and the Cebeci–Smith [18] turbulence model, modified for the wake part of the calculation. Other related computations of interest are by Inouye, Marvin and Sheaffer [19], Cebeci, Stewartson and Whitelaw [20], Bradshaw [21] and Hoffman and Ny [22], for instance, with further studies being listed in the references above.

As far as we know, little or no attention has been given previously to making comparisons between experiments, computations and asymptotic theory as regards the whole turbulent boundary-layer and wake motion for the flat-plate geometry. Mostly, local comparisons close to the trailing edge have been made instead, with Bogucz and Walker [16] in particular summarizing the findings there and providing some interesting remarks on the experimental accuracy or lack of it. The possibility of making fuller, or rather more global, comparisons in the boundary layer and wake motivates the present theoretical study, on asymptotic features, which supposes two-dimensional, symmetric, steady turbulent flow of an incompressible fluid and, perhaps of more significance, takes a specific turbulence model from the outset, namely the Cebeci-Smith algebraic eddy-viscosity one.

There are two extra reasons for the current investigation. The first concerns the issue of whether the specific turbulence model chosen can adequately account for the wake motion or not, and, if so, how accurately, given that the model was proposed originally for wall boundary-layer flows. Doubts have been expressed over the existence of an acceptable wake solution when a model of the Cebeci–Smith kind is used, and especially over the formation of an apparent "cusp" in the inner velocity profile as opposed to the wake symmetry condition. Part of our aim therefore is to discover if acceptable solutions are indeed possible with our procedure and, then, to ask if they are physically sensible and accurate. The second reason is that an increased understanding of wake-flow and trailing-edge effects may well lead on to an understanding of the process of turbulent separation, a process whose structure is so far unclear. The trailing edge forces an abrupt change in boundary conditions and hence in the flow structure, due to the sudden removal of wall shear, and it is found here (see the next paragraph) that the "logarithmic" zone of the turbulent oncoming boundary layer is quickly wiped out in the wake, to be replaced by a new "cuspidal" zone. A similar change in character is believed to occur during turbulent separation, e.g., see the experiments of Trupp, Azad and Kassab [23]. It may be of course that, as some researchers have argued, a severe modification of the turbulence-closure model is inherent during the separation process, but that need not necessarily be so since the analogous present problem involving trailing-edge flow produces marked changes in the flow response even though the turbulence-closure model is unchanged throughout. Turbulent separation is the subject of subsequent work by the present authors [24, 25], work which differs from both the theoretical approaches of Sychev and Sychev [13] and Sychev [14] in the treatment of the outer tier of the turbulent boundary layer prior to separation. We note, again in passing, that the proposed analogy between trailing-edge flow properties and the separation phenomenon works perfectly in laminar flow, as described by Messiter [26] and Stewartson [27] and reviewed recently by Messiter [28] and Smith [29], and indeed there must surely be a strong connection between

the two due to the natural emergence of separation in the trailing-edge regions as a trailing edge is made blunter or at increased angles of attack.

The report is laid out as follows. Section 2 presents the governing equations in a suitably normalized dimensionless form, for the turbulent boundary layer and wake, based on the Cebeci–Smith model. The equations are taken in a boundary-layer version for convenience although the Appendix A shows that the same results emerge from the Navier–Stokes version, to our order of working. Sections 3, 4 then address the boundary-layer and wake features, in turn, when the Reynolds number $\mathrm{Re} = u_\infty l_\infty / \nu$ is large, where u_∞ is the uniform freestream speed, l_∞ is the plate length and ν is the kinematic viscosity of the fluid. The turbulent wake turns out to have a structure rather different from that of the boundary layer. The logarithmic behaviour in the latter is destroyed in the wake because of the reduced maximum stresses acting there and instead a thickened inner tier is induced, with width of the order $\mathrm{Re}^{-2/3}(\ln \mathrm{Re})^{1/3} l_\infty$, giving rise to a "cusp" in the velocity profile just outside this inner tier. The symmetry condition is satisfied, even so, at the wake centre-line which is buried inside that inner tier; thus previous workers' objections to the formation of a cusp are shown to be unfounded. The resulting analytical and numerical predictions for the boundary layer and the wake are compared with experimental findings and fully computational results in Section 5. The agreement in terms of the wake centre-line velocity and the boundary-layer and wake displacement thicknesses is found to be good quantitatively as well as qualitatively. Further discussion is presented in Section 6, including some extra comparisons and conclusions of a more qualitative or structural nature and the generalization to other turbulence models. On this last matter, the present approach is in fact more general than might have been anticipated, since the new wake structure found requires relatively little detailed knowledge of the turbulence model.

The Appendices A–C deal with certain additional aspects arising, Appendix B specifically being concerned with the interactive flow structure surrounding the trailing edge where the erosion of the logarithmic layer takes places quickly and is virtually complete on entry into the full wake of Section 4. Finally here, we note that the velocity components are written u_D, v_D in the x_D, y_D Cartesian directions respectively, where the leading and trailing edges are at (0, 0), (l_∞, 0) respectively, the pressure and the fluid density are p_D, ϱ in turn, and the subscript D where used denotes a dimensional quantity.

2. The governing equations

Two main options for the governing equations of the turbulent boundary layer and wake are addressed in this report. The one we consider mostly is based on the boundary-layer or so-called thin shear layer (TSL) equations, e.g. Cebeci et al. [17],

$$\frac{\partial u_D}{\partial x_D} + \frac{\partial v_D}{\partial y_D} = 0, \tag{2.1}$$

$$u_D \frac{\partial u_D}{\partial x_D} + v_D \frac{\partial u_D}{\partial y_D} = \frac{\partial}{\partial y_D}\left[B_D \frac{\partial u_D}{\partial y_D}\right] + \nu \frac{\partial^2 u_D}{\partial y_D^2} \tag{2.2}$$

in dimensional terms. Here the Cebeci–Smith turbulence model is assumed, in which

$$B_D = \begin{cases} a_1 y_D^2 \left\{1 - \exp\left(\frac{-y_D u_{\tau D}}{a_2 \nu}\right)\right\}^2 \left|\frac{\partial u_D}{\partial y_D}\right| & \text{for } y_D < y_{D1} \quad (2.3a) \\ a_3 u_\infty \delta_D^* & \text{for } y_D > y_{D1}, \quad (2.3b) \end{cases}$$

the constants have the values $a_1 = 0.16$, $a_2 = 26$, $a_3 = 0.0168$, while

$$\delta_D^*(x_D) = \int_0^\infty \left(1 - \frac{u_D}{u_\infty}\right) dy_D \quad (2.3c)$$

is the local displacement thickness, and at the unknown junction $y_D = y_{D1}(x)$ between (2.3a,b) continuity of B, u_D, $\partial u_D/\partial y_D$, i.e., of the eddy viscosity, the velocity and the shear, must be ensured. Again, the unknown friction velocity $u_{\tau D}$ is related to the unknown shear stress on the plate:

$$u_{\tau D} = \left[\nu \frac{\partial u_D}{\partial y_D}(x_D, 0)\right]^{1/2}. \quad (2.3d)$$

The appropriate boundary conditions are

$$u_D = v_D = 0 \quad \text{at} \quad y_D = 0, \quad (2.4a)$$

$$u_D \to u_\infty \quad \text{as} \quad y_D \to \infty, \quad (2.4b)$$

for no slip on the plate and to match with the uniform external stream u_∞, respectively, and the starting condition at $x_D = 0$ is essentially that δ_D^* is zero there. The second option is to address the full Navier–Stokes equations; this option is discussed in Appendix A and is found to yield virtually the same results as those below based on the TSL equations (2.1)–(2.4b), the differences in fact being negligible to our order of working.

Before proceeding with the analysis of the TSL equations we express them in a suitably normalized nondimensional form by setting

$$(u_D, v_D, x_D, y_D) = (u_\infty u, a_1 u_\infty v, l_\infty x, a_1 l_\infty y), \quad R = u_\infty l_\infty a_1^2/\nu \quad (2.5)$$

where $R = a_1^2 \mathrm{Re}$ is a normalized Reynolds number. Then the TSL equations become

$$\frac{\partial u}{\partial x} + \frac{\partial v}{\partial y} = 0, \quad (2.6a)$$

$$u\frac{\partial u}{\partial x} + v\frac{\partial u}{\partial y} = \frac{\partial}{\partial y}\left[B\frac{\partial u}{\partial y}\right] + R^{-1}\frac{\partial^2 u}{\partial y^2}, \quad (2.6b)$$

with B defined by

$$B = \begin{cases} y^2\{1 - \exp(-a_4 R u_\tau y)\}^2 \left|\dfrac{\partial u}{\partial y}\right| & \text{for } y < y_1 \quad (2.6c) \\ a_5\delta \quad \text{for } y > y_1 \quad (2.6d) \end{cases}$$

and

$$\delta(x) = \int_0^\infty (1 - u)\,dy, \quad u_\tau = \left[R^{-1}\frac{\partial u}{\partial y}(x, 0)\right]^{1/2}, \quad (2.6e)$$

$$u = v = 0 \quad \text{at} \quad y = 0\ (0 < x < 1), \quad (2.6f)$$

$$u \to 1 \quad \text{as} \quad y \to \infty, \quad (2.6g)$$

subject also to continuity of B, u, $\partial u/\partial y$ at $y = y_1(x)$. The new constants here are $a_4 = a_2^{-1}a_1^{-1/2}(=0.09615\ldots)$ and $a_5 = a_3a_1^{-1}(=0.105)$, and we note for later reference that $u_\tau = a_1^{-1/2}u_{\tau D}/u_\infty$, $\delta = \delta_D^*/(l_\infty a_1)$ relate the normalised friction velocity and displacement thickness to their dimensional counterparts introduced earlier. The system (2.6a–g) describing the turbulent boundary layer $0 < x < 1$ and the turbulent wake $x > 1$ (with symmetry at $y = 0$ replacing (2.6f)) is analysed below for large Reynolds numbers R, with an alternative treatment being summarised in Appendix A.

3. The boundary layer

The classical boundary layer for $0 < x < 1$ has the structure indicated by Mellor [5] and Bush and Fendell [6], at large Reynolds numbers. It takes on a two-tiered form I, II (see Fig. 1(a)), in which the outer tier I has thickness y of order ε and involves only a small deficit of order ε in the velocity u from its freestream value of unity, whereas in the inner tier II

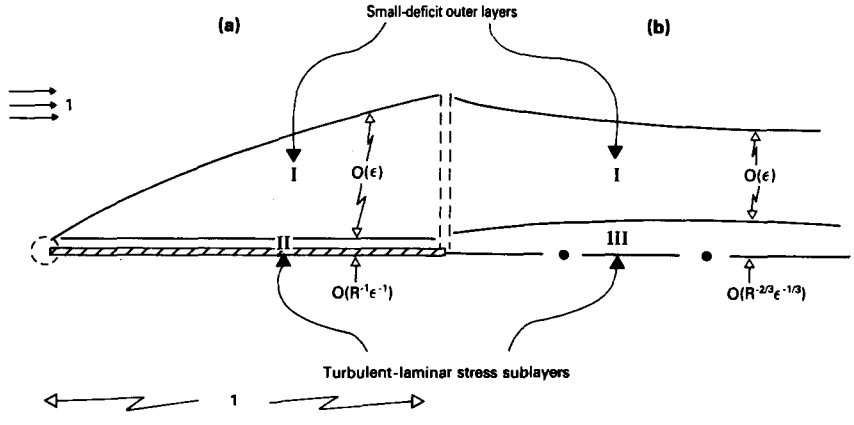

Fig. 1. The general flow structure for (a) the turbulent boundary layer and (b) the wake at high Reynolds numbers R, showing the main regions I–III of Sections 3, 4. In (a), layers I, II merge via a logarithmic velocity deficit, while in (b) layers I, III merge via a cuspidal velocity deficit. The extra regions close to the trailing edge are presented in Fig. 5 and Appendix B.

of thickness $O(R^{-1}\varepsilon^{-1})$, very close to the plate, u is reduced to $O(\varepsilon)$. The merging between the two tiers is achieved by means of logarithmic behaviour in the velocity deficit in I and the velocity in II. Here the parameter

$$\varepsilon \equiv (\ln R)^{-1} \tag{3.1}$$

is small, since $R \gg 1$, and u_τ is also of order ε.

In the small-deficit outer layer I, where the major balance of forces is between inertia and turbulent shear stress, the velocity field expands as

$$u = 1 + \varepsilon u_1 + \varepsilon^2(\ln \varepsilon)u_{2L} + \varepsilon^2 u_2 + \ldots, \tag{3.2a}$$

$$v = \varepsilon^2 v_1 + \varepsilon^3(\ln \varepsilon)v_{2L} + \varepsilon^3 v_2 + \ldots, \tag{3.2b}$$

with $y = \varepsilon\bar{y}$ and $\bar{y}$ is O(1). This implies that the displacement thickness δ in (2.6e) now has the form

$$\delta = \varepsilon^2\delta_1 + \varepsilon^3(\ln \varepsilon)\delta_{2L} + \varepsilon^3\delta_2 + \ldots. \tag{3.2c}$$

Strictly the unknown junction position $y = y_1(x)$ should also be expanded asymptotically but the setting $y_1 = \varepsilon\bar{y}_1$ is sufficient for present purposes, e.g. for determining the displacement thickness to order ε^3. From substitution into the TSL equations (2.6) the successive governing equations obtained are as follows. First, u_1, v_1 are controlled by the inertia-vs.-turbulent-stress equations

$$\frac{\partial u_1}{\partial x} + \frac{\partial v_1}{\partial \bar{y}} = 0, \tag{3.3a}$$

$$\frac{\partial u_1}{\partial x} = \begin{cases} \dfrac{\partial}{\partial \bar{y}}\left[\bar{y}^2\left(\dfrac{\partial u_1}{\partial \bar{y}}\right)^2\right] & \text{for } \bar{y} < \bar{y}_1, \\ a_5\delta_1 \dfrac{\partial^2 u_1}{\partial \bar{y}^2} & \text{for } \bar{y} > \bar{y}_1, \end{cases} \tag{3.3b}$$

since here $B \approx \varepsilon^2\bar{y}^2\,|\partial u_1/\partial\bar{y}|$ or $\varepsilon^2 a_5\delta_1$ to leading order and we expect the shear $\partial u/\partial y$ to be positive throughout, an assumption that can be justified *a posteriori*. Again,

$$\delta_1 = -\int_0^\infty u_1\,d\bar{y}. \tag{3.3c}$$

The boundary conditions relevant at this stage are

$$u_1 \to 0 \text{ as } \bar{y} \to \infty,\ u_1 \sim \ln \bar{y} + O(1) \text{ as } \bar{y} \to 0+, \tag{3.3d}$$

the former coming from the freestream condition (2.6g) and the latter from the matching discussed a little later: see (3.11a, b) below. The solution of (3.3a–d) is required to determine

in particular the unknown velocity-deficit function $k_1(x)$, where

$$u_1 \sim \ln \bar{y} + k_1(x) + O(\bar{y}) \quad \text{as} \quad \bar{y} \to 0+ \tag{3.4}$$

from an extension of (3.3d). Second, for u_{2L}, v_{2L} we have the governing equations

$$\frac{\partial u_{2L}}{\partial x} + \frac{\partial v_{2L}}{\partial \bar{y}} = 0, \tag{3.5a}$$

$$\frac{\partial u_{2L}}{\partial x} = \begin{cases} 2 \dfrac{\partial}{\partial \bar{y}} \left[\bar{y}^2 \dfrac{\partial u_1}{\partial \bar{y}} \dfrac{\partial u_{2L}}{\partial \bar{y}} \right] & \text{for} \quad \bar{y} < \bar{y}_1, \\ a_5 \left(\delta_1 \dfrac{\partial^2 u_{2L}}{\partial \bar{y}^2} + \delta_{2L} \dfrac{\partial^2 u_1}{\partial \bar{y}^2} \right) & \text{for} \quad \bar{y} > \bar{y}_1, \end{cases} \tag{3.5b}$$

from (2.6a–d), along with

$$\delta_{2L} = -\int_0^\infty u_{2L} \, d\bar{y}, \tag{3.5c}$$

$$u_{2L} \to 0 \quad \text{as} \quad \bar{y} \to \infty, \quad u_{2L} \sim -2 \ln \bar{y} \quad \text{as} \quad \bar{y} \to 0+ \tag{3.5d}$$

– again see (3.11) below. Third, the controlling equations for u_2, v_2 are

$$\frac{\partial u_2}{\partial x} + \frac{\partial v_2}{\partial \bar{y}} = 0, \tag{3.6a}$$

$$\frac{\partial u_2}{\partial x} + u_1 \frac{\partial u_1}{\partial x} + v_1 \frac{\partial u_1}{\partial \bar{y}} = \begin{cases} 2 \dfrac{\partial}{\partial \bar{y}} \left[\bar{y}^2 \dfrac{\partial u_1}{\partial \bar{y}} \dfrac{\partial u_2}{\partial \bar{y}} \right] & \text{for} \quad \bar{y} < \bar{y}_1, \\ a_5 \left(\delta_1 \dfrac{\partial^2 u_2}{\partial \bar{y}^2} + \delta_2 \dfrac{\partial^2 u_1}{\partial \bar{y}^2} \right) & \text{for} \quad \bar{y} > \bar{y}_1, \end{cases} \tag{3.6b}$$

where

$$\delta_2 = -\int_0^\infty u_2 \, d\bar{y} \tag{3.6c}$$

and

$$u_2 \to 0 \quad \text{as} \quad \bar{y} \to \infty, \quad u_2 \sim (k_1 - k_2) \ln \bar{y} \quad \text{as} \quad \bar{y} \to 0+, \tag{3.6d}$$

again from the freestream condition and from the matching in (3.11) below. The starting conditions at the leading edge $x = 0$ are $\delta_1(0) = \delta_{2L}(0) = \delta_2(0) = 0$. Also, the extra unknown function $k_2(x)$ appearing in (3.6d) is to be determined by the behaviour in the viscous sublayer II below, and the junction position $y_1 \approx \varepsilon \bar{y}_1$ is assumed to be typically of order ε.

The inner sublayer II, by contrast, involves a balance between the turbulent and laminar viscous stresses alone. In II we have $y = R^{-1}\varepsilon^{-1}\tilde{y}$, with $\tilde{y}$ now of O(1), and

$$u = \varepsilon\tilde{u} + O(\varepsilon^2 \ln \varepsilon). \tag{3.7}$$

Thus the main governing equation here is, from (2.6b),

$$0 = \frac{\partial}{\partial\tilde{y}}\left[\tilde{y}^2\{1 - \exp(-a_6\tilde{y})\}^2\left(\frac{\partial\tilde{u}}{\partial\tilde{y}}\right)^2\right] + \frac{\partial^2\tilde{u}}{\partial\tilde{y}^2} \tag{3.8a}$$

subject to the constraints

$$\tilde{u} \sim \ln\tilde{y} \quad \text{as} \quad \tilde{y} \to \infty, \quad \tilde{u} = 0 \quad \text{at} \quad \tilde{y} = 0, \tag{3.8b,c}$$

to merge with the solution in layer I and to satisfy (2.6f), in turn. In (3.8a) to leading order $a_6 \equiv a_4 u_\tau \varepsilon^{-1}$ is O(1). A first integral of (3.8a) gives

$$\tilde{y}^2\{1 - \exp(-a_6\tilde{y})\}^2\left(\frac{\partial\tilde{u}}{\partial\tilde{y}}\right)^2 + \frac{\partial\tilde{u}}{\partial\tilde{y}} = 1, \tag{3.9a}$$

however, in view of the requirement that $\partial\tilde{u}/\partial\tilde{y} \sim \tilde{y}^{-1}$ as $\tilde{y} \to \infty$, from (3.8b), and hence $\partial\tilde{u}/\partial\tilde{y} = 1$ at the plate $\tilde{y} = 0$, so that (2.6e) gives $u_\tau = \varepsilon$ to leading order. Therefore $a_6 = a_4$. Next, (3.9a) can be solved for the shear stress,

$$\frac{\partial\tilde{u}}{\partial\tilde{y}} = \frac{-1 + [1 + 4\tilde{y}^2\{1 - \exp(-a_4\tilde{y})\}^2]^{1/2}}{2\tilde{y}^2\{1 - \exp(-a_4\tilde{y})\}^2}, \tag{3.9b}$$

after which the sublayer velocity is fixed by

$$\tilde{u} = \int_0^{\tilde{y}} \frac{\partial\tilde{u}}{\partial\tilde{y}}\,\mathrm{d}\tilde{y}, \tag{3.9c}$$

from (3.8c). Hence we obtain the asymptote

$$\tilde{u} \sim \ln\tilde{y} + k_2(x) \quad \text{as} \quad \tilde{y} \to \infty, \tag{3.9d}$$

say, where the function $k_2(x)$ is given by

$$k_2(x) = \lim_{\tilde{y}\to\infty}\left\{\int_0^{\tilde{y}}\left(\frac{[1 + 4q^2\{1 - \exp(-a_4q)\}^2]^{1/2} - 1}{2q^2\{1 - \exp(-a_4q)\}^2}\right)\mathrm{d}q - \ln\tilde{y}\right\} \tag{3.9e}$$

and in fact is constant. It is noted here also that the friction velocity u_τ has the form

$$u_\tau = \varepsilon + \varepsilon^2(\ln\varepsilon)u_{\tau 2L} + \varepsilon^2 u_{\tau 2} + \ldots, \tag{3.10}$$

for later reference.

The merging between the two tiers I, II anticipated above perhaps needs a little clarification now. If the more general forms

$$u_1 \sim h_1 \ln \bar{y} + k_1,\ u_{2L} \sim h_{2L} \ln \bar{y} + \mathrm{O}(1),\ u_2 \sim h_2 \ln \bar{y} + \mathrm{O}(1) \tag{3.11a}$$

hold in tier I, as $\bar{y} \to 0+$, then the velocity implied by tier I becomes

$$\begin{aligned} u \;=\; & 1 + \varepsilon[h_1(-\ln R - 2\ln \varepsilon + \ln \tilde{y}) + k_1] + \varepsilon^2 \ln \varepsilon[h_{2L}(-\ln R) + \mathrm{O}(\ln \varepsilon)] \\ & + \varepsilon^2[h_2(-\ln R) + \mathrm{O}(\ln \varepsilon)] \end{aligned} \tag{4.11b}$$

as the inner tier II is entered, i.e. as $\bar{y} \to R^{-1}\varepsilon^{-2}\tilde{y}$. To match with tier II's velocity in (3.7), therefore, given ε in (3.1), the contributions of orders 1, $\varepsilon \ln \varepsilon$ and ε in (3.11b) demand, in turn, the relations $h_1 = 1$, $h_{2L} = -2h_1$, $-h_2 + k_1 = k_2$ and that $\tilde{u} \sim h_1 \ln \tilde{y} + k_2$ as $\tilde{y} \to \infty$. Hence the constraints involving logarithms in (3.3d), (3.4), (3.5d), (3.6d), (3.8b), (3.9d) are all verified.

The main results we require from the working are the unknown displacement contributions in (3.2c). The first one, $\delta_1(x)$, can be deduced from integration of (3.3b) with respect to $\bar{y}$, from zero to infinity, yielding

$$-\frac{\mathrm{d}\delta_1}{\mathrm{d}x} \;=\; -\lim_{\bar{y}\to 0+}\left[\bar{y}^2\left(\frac{\partial u_1}{\partial \bar{y}}\right)^2\right] \;=\; -1$$

in view of (3.3c,d). Hence, as $\delta_1(0) = 0$,

$$\delta_1 \;=\; x. \tag{3.12}$$

The second contribution, $\delta_{2L}(x)$, likewise follows from direct integration of (3.5b), which gives

$$-\frac{\mathrm{d}\delta_{2L}}{\mathrm{d}x} \;=\; -\lim_{\bar{y}\to 0+}\left[2\bar{y}^2\frac{\partial u_1}{\partial \bar{y}}\frac{\partial u_{2L}}{\partial \bar{y}}\right] \;=\; 4$$

on use of (3.3d), (3.5d), so that

$$\delta_{2L} \;=\; -4x. \tag{3.13}$$

The third contribution $\delta_2(x)$ is rather trickier to evaluate. For integration of (3.6b) across the layer now gives

$$-\frac{\mathrm{d}\delta_2}{\mathrm{d}x} + \frac{\mathrm{d}}{\mathrm{d}x}\int_0^\infty u_1^2\,\mathrm{d}\bar{y} \;=\; -\lim_{\bar{y}\to 0+}\left[2\bar{y}^2\frac{\partial u_1}{\partial \bar{y}}\frac{\partial u_2}{\partial \bar{y}}\right] \;=\; -2(k_1 - k_2), \tag{3.14}$$

from (3.3a,d) with (3.6d), and so the detailed properties of $u_1(x, \bar{y})$ are needed here. Fortunately the solution for u_1 is of the similarity type, specifically

$$u_1 \;=\; f_1(\eta) \quad \text{with} \quad \eta \;=\; \bar{y}/x \tag{3.15a}$$

where, from (3.3b,d), f_1 satisfies

$$-\eta f_1' = \begin{cases} (\eta^2 f_1'^2)' \text{ (for } \eta < \eta_1) \\ a_5 f_1'' \quad \text{(for } \eta > \eta_1) \end{cases} \tag{3.15b}$$

since $\delta_1 = x$, and the junction $\bar{y}_1 = x\eta_1$ say, subject to

$$f_1(\infty) = 0, \quad f_1 \sim \ln \eta + O(1) \quad \text{as} \quad \eta \to 0+. \tag{3.15c}$$

The solution is

$$f_1 = \begin{cases} \ln \eta + b_1 - \eta/2 \quad \text{for} \quad 0 < \eta < \eta_1 \\ c_1 \int_\infty^\eta \exp\left((\eta_1^2 - \eta^2)/2a_5\right) d\eta \quad \text{for} \quad \eta > \eta_1 \end{cases} \tag{3.16a}$$

where continuity of f_1, f_1' and stress, i.e, $\eta^2 f_1' = a_5$, at $\eta = \eta_1$, imposes the three conditions

$$\begin{aligned} \ln \eta_1 + b_1 - \eta_1/2 &= -c_1 \int_{\eta_1}^\infty \exp\left((\eta_1^2 - \eta^2)/2a_5\right) d\eta, \\ \eta_1^{-1} - \tfrac{1}{2} &= c_1, \\ \eta_1 - \eta_1^2/2 &= a_5, \end{aligned} \tag{3.16b}$$

necessary to fix the three unknown constants η_1, b_1, c_1. We find from (3.16b) that

$$\eta_1 = 1.889, \quad b_1 = 0.307, \quad c_1 = 0.0294 \tag{3.16c}$$

and hence the velocity function k_1 is determined as

$$k_1(x) = -\ln x + b_1. \tag{3.16d}$$

Returning to (3.14), therefore, and integrating, we obtain the displacement correction δ_2 in the form

$$\delta_2(x) = x\left\{\int_0^\infty f_1^2 \, d\eta - 2k_2 + 2 + 2b_1\right\} - 2x \ln x, \tag{3.17}$$

since k_2 is constant. Furthermore, numerical evaluation of the integral appearing in (3.17) gives its value as 1.68, while computation of (3.9e) yields the value $k_2 = 3.01$, using trapezoidal rules coupled with grid-size extrapolation.

Combining these results, we derive the prediction

$$\delta(x) = \varepsilon^2 x - 4\varepsilon^3 (\ln \varepsilon) x + \varepsilon^3 [(-1.74)x - 2x \ln x] \tag{3.18}$$

for the normalized displacement thickness of the boundary layer, for $0 < x < 1$, when the Reynolds number is large. This is compared with experimental and fully numerical findings in Section 5.

4. The wake

Our procedure for the turbulent symmetric wake $x > 1$ is to continue with the TSL equations of Section 2 unchanged, i.e., to keep the Cebeci–Smith model, although with symmetry conditions along the centre line of course, and then see if a sensible structure, governing equations and predictions emerge for the entire wake flow.

Thus (2.6a–e,g) continue to hold in the wake but with (2.6f) replaced by

$$\frac{\partial u}{\partial y} = v = 0 \quad \text{at} \quad y = 0 \text{ (for } x > 1). \tag{4.1}$$

Then for large Reynolds numbers the approach in (3.1)–(3.2c) still applies exactly for the outer bulk I of the wake, of thickness $O(\varepsilon)$, wherein $\bar{y}$ is O(1) and the junction $y_1 \approx \varepsilon\bar{y}_1$ is situated. So at leading order the governing equations for u_1, v_1 are again (3.3a,b), subject again to (3.3c) and to the first constraint in (3.3d), that u_1 vanishes as $\bar{y} \to \infty$. The second constraint in (3.3d) concerning logarithmic behaviour no longer applies now, however, for the following reason. It would require an inner shear-stress layer (II) just as in (3.7) above, leading then to (3.8a,b) but with $\partial\tilde{u}/\partial\tilde{y} = 0$ at $\tilde{y} = 0$ instead of (3.8c), because of the symmetry condition (4.1). Integration of (3.8a) with respect to $\tilde{y}$ and application of (3.8b) would therefore reproduce the result (3.9a) and this would contradict the centre-line constraint $\partial\tilde{u}/\partial\tilde{y} = 0$ at $\tilde{y} = 0$. The resolution is that the logarithmic term in u_1 as $\bar{y} \to 0+$ must be absent in the wake, i.e.

$$u_1 = o(\ln \bar{y}) \quad \text{as} \quad \bar{y} \to 0+, \tag{4.2a}$$

and it is found (see below and Fig. 1(b)) that the thin inner layer II is no longer present, being replaced by a new thicker layer III. The only way for (4.2a) to be achieved, in fact, is if the small-$\bar{y}$ behaviour of u_1 has the form

$$u_1 = q_1(x) + 2(q_1'(x))^{1/2}\bar{y}^{1/2} + O(\bar{y}) \quad \text{as} \quad \bar{y} \to 0+, \tag{4.2b}$$

from substitution into the controlling equation (3.3b). This supposes that the centre-line correction velocity $q_1(x)$ increases monotonically with $x(q_1' \geqslant 0)$, which is found to be true subsequently: see Fig. 2 below. It supposes also that the $\bar{y}^{1/2}$ response or "cusp" appearing in the velocity profile in (4.2b), and to which reference was made in the introduction, can be eradicated in an inner sublayer, III say, nearer the centre line in order to avoid contradicting the symmetry condition (4.1). The required sublayer III is considered next.

The size of the new inner layer III stems from an order-of-magnitude estimate. The shear $\partial u/\partial y \sim \bar{y}^{-1/2}[= \varepsilon^{1/2}y^{-1/2}]$ for small $\bar{y}$, from (4.2b) coupled with (3.2a), and so a new turbulent-laminar stress balance comes into force when $\varepsilon y \sim R^{-1}\varepsilon^{1/2}y^{-1/2}$, from balancing the term $y^2(\partial u/\partial y)^2$ against the term $R^{-1}(\partial u/\partial y)$ in (2.6b), i.e., when $y \sim R^{-2/3}\varepsilon^{-1/3}$. At that stage the inertia term also balances the shear-stress contributions, as indeed (4.2b) implies since the response (4.2b) relies on inertial and turbulent-stress effects remaining comparable. Hence the sublayer III has $y = R^{-2/3}\varepsilon^{-1/3}\hat{y}$ say, with $\hat{y}$ of O(1) typically, v is $O(R^{-2/3}\varepsilon^{2/3})$ and

$$u = 1 + \varepsilon q_1(x)\{+ \ldots\} + R^{-1/3}\varepsilon^{1/3}\hat{u}(x, \hat{y}) + \cdots \tag{4.3}$$

where the intervening terms $\{+ \ldots\}$ are independent of $\hat{y}$: see e.g., (4.6)ff below. From (2.6b) the main governing equation here is

$$q_1'(x) = \frac{\partial}{\partial \hat{y}}\left[\hat{y}^2\left(\frac{\partial \hat{u}}{\partial \hat{y}}\right)^2\right] + \frac{\partial^2 \hat{u}}{\partial \hat{y}^2}, \tag{4.4a}$$

expressing an interplay of inertial, turbulent and laminar stresses as anticipated. We observe also that this inner-wake layer III is much thicker [$O(R^{-2/3}\varepsilon^{-1/3})$] than the classical $O(R^{-1}\varepsilon^{-1})$ inner-wall zone II of the boundary layer on the plate, and moreover it does not depend on the precise details of the turbulence model in (2.6c), only on the outer part $y^2|\partial u/\partial y|$ in B there, unlike the inner-wall zone II of (3.8a)–(3.9e). The constraints on (4.4a) are

$$\hat{u} \sim 2(q_1')^{1/2}\hat{y}^{1/2} \quad \text{as} \quad \hat{y} \to \infty, \qquad \frac{\partial \hat{u}}{\partial \hat{y}} = 0 \quad \text{at} \quad \hat{y} = 0, \tag{4.4b,c}$$

due to (4.2b), (4.1) respectively. Consequently the $\hat{y}$-integral of (4.4a), subject to (4.4c), gives

$$\hat{y}^2\left(\frac{\partial \hat{u}}{\partial \hat{y}}\right)^2 + \frac{\partial \hat{u}}{\partial \hat{y}} = \hat{y}q_1', \tag{4.4d}$$

so that

$$\hat{\tau} \equiv \frac{\partial \hat{u}}{\partial \hat{y}} = [(1 + 4\hat{y}^3 q_1')^{1/2} - 1]/2\hat{y}^2, \quad \hat{u} = \int_0^{\hat{y}} \hat{\tau}\, d\hat{y} + \hat{u}(x, 0). \tag{4.4e,f}$$

The condition (4.4b) is met, therefore, since $\hat{\tau} \sim (q_1')^{1/2}\hat{y}^{-1/2}$ for large $\hat{y}$ from (4.4e), and so the sublayer III's solution acts as required to smooth out the cusp in the velocity-profile behaviour (4.2b) and to ensure the full symmetry condition along the centre line. No distinct sublayer thinner than III appears necessary, by the way.

Our primary task, then, to determine the turbulent wake properties, is to solve the outer-layer problem (3.3b) for u_1 in $x > 1$ subject to (3.3c), $u_1(x, \infty) = 0$ and (4.2b), and with the starting form

$$u_1(1, \bar{y}) = f_1(\bar{y}) \quad \text{for} \quad 0 < \bar{y} < \infty \tag{4.5}$$

where the trailing-edge profile f_1 is specified in Section 3; see (3.16a–c). Before describing the solution we remark that the centre-line velocity is predicted here to be

$$u_{CL} \equiv u(x, 0) = 1 + \varepsilon q_1(x) + O(\varepsilon^2 \ln \varepsilon) \tag{4.6}$$

from (4.2b), where $q_1(x)$ is to be found, and in principle further terms in (4.6) can also be found from the solution of the successive problems for u_{2L}, u_2 and so on, including the small contribution from $\hat{u}(x, 0)$ in (4.3). For example, u_{2L}, u_2 satisfy (3.5b, c), (3.6b, c) again but the inner constraints for the wake $x > 1$ are that u_{2L}, u_2 remain finite at $\bar{y} = 0$, as opposed to (3.5d) (3.6d). Thus, as with (4.2b), the logarithmic law and the so-called logarithmic layer, between tiers I, II on the plate, are wiped out in the wake motion. Further, the displacement

contributions δ_1, δ_{2L}, δ_2 can be worked out by integrating the momentum equations for $u_{1,2L,2}$ across the wake and due to the disappearance of the logarithmic responses just mentioned, we obtain the simple results $\mathrm{d}\delta_1/\mathrm{d}x = \mathrm{d}\delta_{2L}/\mathrm{d}x = 0$, $\mathrm{d}\delta_2/\mathrm{d}x = \mathrm{d}J/\mathrm{d}x$, in contrast with (3.12)–(3.14). Here J is the integral of u_1^2 across the half-wake. Since $\delta_{1,2L,2}$ are continuous at the trailing edge, therefore

$$\delta_1 = 1, \quad \delta_{2L} = -4, \quad \delta_2 = J(x) + \{\delta_2(1) - J(1)\} \tag{4.7a}$$

for $x > 1$, where

$$J(x) \equiv \int_0^\infty u_1^2 \, \mathrm{d}\bar{y}; \tag{4.7b}$$

the displacement thickness of the wake then follows from (3.2c). Hence the outer-layer solution for $u_1(x, \bar{y})$, addressed next in (a)–(c), is needed mainly for the evaluation of the contributions $q_1(x)$ in the centre-line velocity and $J(x)$ in the displacement thickness.

(*a*) *The near-wake*, just beyond the trailing edge at $x = 1$, provides some useful information first. Across most of the outer layer I the velocity u_1 expands regularly, for example

$$u_1 = f_1(\bar{y}) + (x - 1)(\bar{y}^2 f_1'^2)' + \ldots \quad \text{as} \quad x \to 1+ \tag{4.8}$$

below the junction at $\bar{y} = \bar{y}_1$, from substitution of (4.5) into (3.3b), and similarly above the junction. This holds except for small $\bar{y}$ where the behaviour $f_1(\bar{y}) \sim \ln \bar{y}$ (from (3.16a)) violates the wake condition (4.2b), thus calling for a relatively thin inner zone. The inner zone turns out to have thickness $\bar{y}$ of order $(x - 1)$ to preserve a momentum balance and so

$$u_1 = \ln (x - 1) + F_1(\xi) + \ldots \quad \text{as} \quad x \to 1+ \tag{4.9a}$$

with $\xi = \bar{y}/(x - 1)$ of order unity. Substitution into (3.3b) leaves the equation

$$1 - \xi F_1' = (\xi^2 F_1'^2)' \tag{4.9b}$$

for $F_1(\xi)$, with the conditions $F_1 \sim \ln \xi + \mathrm{O}(1)$ as $\xi \to \infty$, to match with (4.8) outside, and $F_1(0)$ to be finite, to comply with (4.2b). Setting $\xi F_1' = \Phi(\xi)$ converts (4.9b) to the form $1 - \Phi = 2\Phi\Phi'$, so that, on integration,

$$\xi = -2\{\Phi + \ln (1 - \Phi)\} \tag{4.9c}$$

fixes the solution implicitly. In (4.9c) the condition $\Phi(0) = 0$ has been used, corresponding to the finiteness requirement on $F_1(0)$. The solution is presented in Fig. 2, and we note that in the upper extremes of this layer $\Phi \sim 1 - \mathrm{e}^{-1} \exp(-\xi/2)(\xi \to \infty)$, giving $F_1' \sim \xi^{-1}$ as necessary, while as the centre line is approached $(\xi \to 0+)\Phi \sim \xi^{1/2}$, so that $F_1 \sim F_1(0) + 2\xi^{1/2}$ there, which complies with the wake condition (4.2b). Indeed, this allows the centre-line velocity contribution $q_1(x)$ to be determined,

$$q_1(x) \sim \ln (x - 1) + e_1 \quad \text{for} \quad x \to 1+, \tag{4.10a}$$

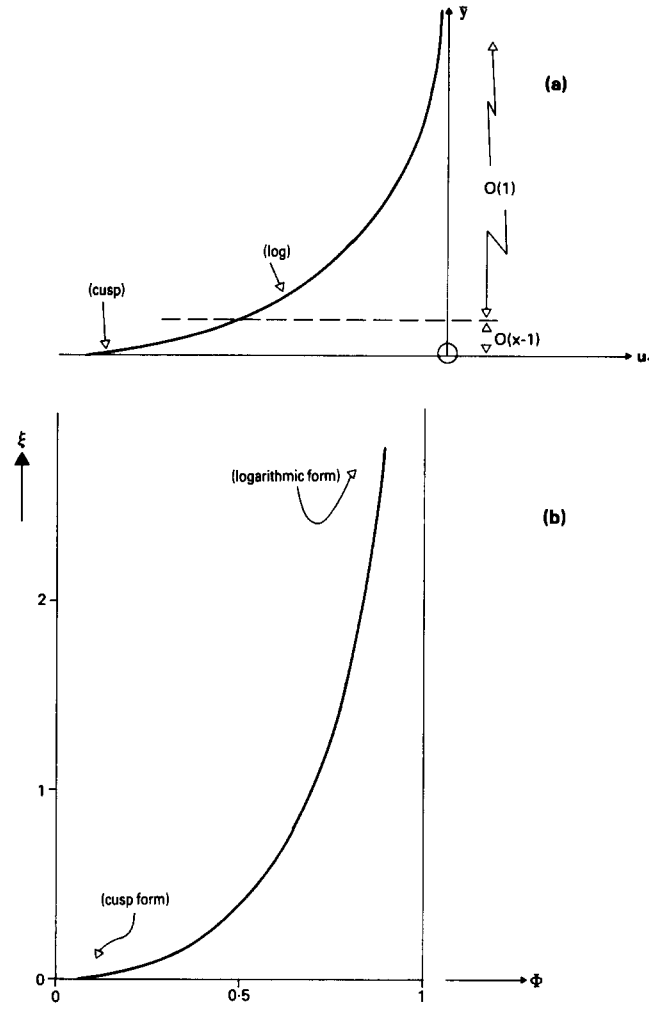

Fig. 2. Properties for the wake flow of Section 4: (a) the near-wake velocity deficit in layer I (sketch); (b) the function $\Phi(\xi)$ appearing in the near-wake solution; (c) centre-line velocity $u_1(x, 0)$ versus x; (d) the displacement contribution J versus x. Asymptotes are as shown. Further computational details are in Appendix C.

where the constant $e_1 = F_1(0)$ is given by

$$e_1 = \lim_{\xi\to\infty}\left\{\ln\xi - \int_0^\xi \xi^{-1}\Phi\,\mathrm{d}\xi\right\} + b_1 = -1.137 \tag{4.10b}$$

since $F_1 = \int_0^\xi \xi^{-1}\Phi\,\mathrm{d}\xi + e_1$ must tend to $\ln\xi + b_1$ for large ξ, with b_1 given in (3.16a,c). We obtained the numerical value in (4.10b) by manipulating the formula for $e_1 - b_1$ into the form

$$\int_0^\infty \ln\{2(e^{-s} - 1 + s)/s^2\}e^{-s}\,\mathrm{d}s - 2\gamma$$

and evaluating the integral here by trapezoidal integration and grid-extrapolation; γ is Euler's constant 0.577215 ....

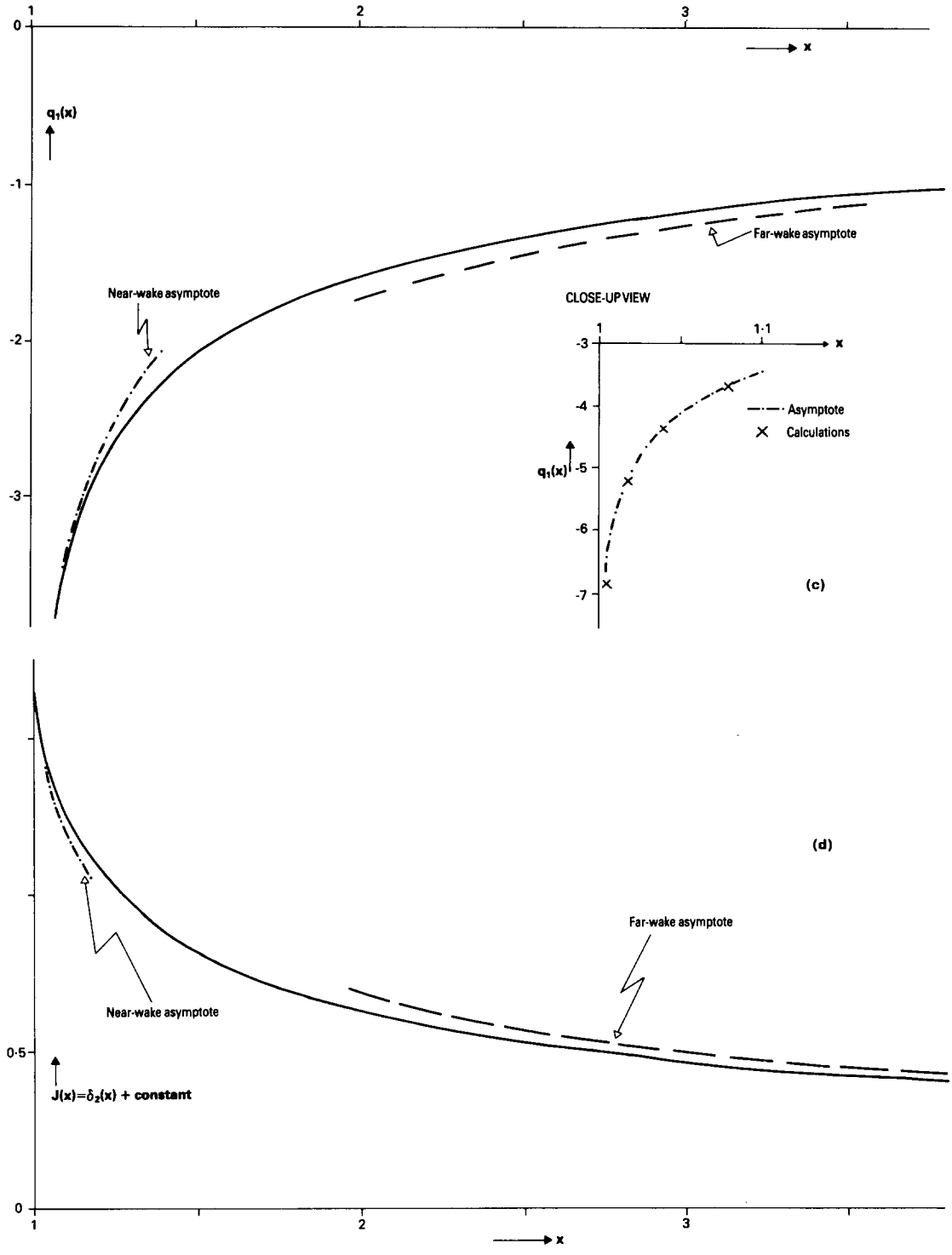

Fig. 2. Continued

The local analysis above also allows the displacement contribution $\delta_2(x)$ in (4.7) to be evaluated just beyond the trailing edge. It is found that

$$\delta_2(x) \sim \delta_2(1) + 2(x-1)\ln(x-1) + O(x-1)\ (x \to 1+), \tag{4.11}$$

with the major contribution to the slope $\delta_2'(x)$ coming from the inner zone where (4.9a) holds. The scaled displacement slope is therefore large and negative for small $(x-1)$, within the present scales.

The marked effects at the start of the wake, regarding the increasingly large negative velocity correction q_1 in (4.10a), the increasingly large negative displacement slope δ_2' due to (4.11), and the splitting of the small-deficit layer I into two parts ($\bar{y} \sim 1$, $\bar{y} \sim x-1$), for small $(x-1)$, lead on to the examination of localized trailing-edge regions in Appendix B. The whole response in the near-wake seems physically sensible, we observe, including all the three features just described, and moreover it is found to be in broad agreement with computations and experimental measurements of wake flows, as discussed later on. Finally here, it is worth re-emphasizing the way the wake motion obliterates the logarithmic behaviour from the velocity profiles. Near the trailing edge that is achieved via the inner zone of (4.9a) and its solution (4.9c), which takes the incoming logarithmic form due to f_1 for large ξ and converts it to the "cusp" form holding nearer the centre line for small ξ (and thence into the sublayer III described previously). On the plate upstream, by contrast, the solution of (4.9b) is simply $\Phi \equiv 1$, giving $F_1 \equiv \ln\xi + b_1$ and producing the logarithmic layer closer to the plate surface.

(*b*) *The far-wake*, for large positive x, develops the similarity form

$$u_1 \sim x^{-1/2} g_1(\hat{\eta}) + \ldots \quad \text{with} \quad \hat{\eta} = \bar{y}x^{-1/2}, \tag{4.12}$$

as the flow there returns to the uniform stream, $u \to 1$. From (3.3b) with (4.7a), g_1 satisfies the nonlinear/linear differential equations

$$-\tfrac{1}{2}g_1 - \tfrac{1}{2}\hat{\eta}g_1' = \begin{cases} (\hat{\eta}^2 g_1'^2)', & \hat{\eta} < \hat{\eta}_1, \\ a_5 g_1'', & \hat{\eta} > \hat{\eta}_1, \end{cases} \tag{4.13a}$$

while the boundary conditions are

$$g_1(0) = \text{finite}, \quad g_1(\infty) = 0 \tag{4.13b}$$

and at the unknown junction $(\hat{\eta} = \hat{\eta}_1)$ g_1, g_1' are to be continuous, with $\hat{\eta}_1^2 g_1' \to a_5$ as $\hat{\eta} \to \hat{\eta}_1 -$. Also, the constant displacement δ_1 in (4.7a) requires that

$$-\int_0^\infty g_1(\hat{\eta})\,\mathrm{d}\hat{\eta} = 1. \tag{4.13c}$$

The equations in (4.13a) yield the solution

$$g_1(\hat{\eta}) = \begin{cases} -\tfrac{1}{2}(\hat{\eta}^{1/2} - \sigma_1)^2 & \text{for } \hat{\eta} < \hat{\eta}_1, \\ \sigma_2 \exp(-\hat{\eta}^2/4a_5) & \text{for } \hat{\eta} > \hat{\eta}_1, \end{cases} \tag{4.14a}$$

and then the constraints between (4.13b,c) provide three independent equations fixing the three unknown constants $\hat{\eta}_1$, σ_1, σ_2. In particular we find $\sigma_1 = 1.861$, which from (4.14a), (4.12), (4.2b) leads to the downstream asymptote

$$q_1(x) \sim -1.73x^{-1/2} \quad \text{as} \quad x \to \infty \tag{4.14b}$$

for the centre-line velocity correction. The far-downstream behaviour of the displacement contribution $\delta_2(x)$ in (4.7a,b) can also be worked out now, from the integral of g_1^2 across the half-wake, producing

$$\delta_2(x) \sim \{\delta_2(1) - \mathrm{J}(1)\} + 0.693\,x^{-1/2} \quad \text{as} \quad x \to \infty. \tag{4.14c}$$

Like the near-wake results in sub-section (a) above, the present results for the far-wake provide useful checks on the calculations discussed subsequently in (c) as well as being physically sensible in themselves and turning out to be in agreement with the experimental wake properties (see Section 5).

(*c*) *The complete wake* properties require a numerical treatment of the governing equation (3.3b) for $x > 1$, subject to (4.2b), (4.5), (4.7a) (replacing (3.3c)) and $u_1(x, \infty) = 0$. This was done with an explicit predictor-corrector finite-difference scheme, of nominally second-order accuracy in x, $\bar{y}$, starting with the profile (4.5) at $x = 1$. The computational scheme is described in detail in Appendix C, together with the checks made on its accuracy, while the results are summarized in Fig. 2.

The principal results are for the centre-line correction velocity q_1 and the displacement term δ_2, versus x. For small $(x - 1)$ the computations agree well with the near-wake analysis in (a) above and appear to capture the predicted irregular response there adequately. As x then increases the velocity $q_1(x)$ continues to increase, while the displacement $\delta_2(x)$ decreases monotonically, throughout the wake, and for large x the downstream responses predicted in (b) above are approached, as expected.

The two conclusions we draw from this section are: first, the original Cebeci-Smith model can indeed be continued into and throughout the turbulent wake, in the sense that a complete wake solution does emerge; and, second, the wake solution found is physically sensible, allowing the flow for example to accelerate along the entire wake and approach the free stream far downstream. Next, therefore, we compare the wake predictions above and those for the boundary layer with experimental and fully computational findings.

5. Comparisons with experiments and computations

Concerning the *boundary-layer* analysis in Section 3, our main prediction is (3.18) for the normalized displacement δ, in $0 < x < 1$, which implies for the displacement thickness δ_D^*

$$\frac{\delta_D^*}{l_\infty} = \varepsilon^2 a_1 x - 4a_1\varepsilon^3 (\ln \varepsilon)x + \varepsilon^3 a_1(-1.74x - 2x \ln x), \tag{5.1}$$

to order ε^3, where $a_1 = 0.16$, $\varepsilon = \{\ln(a_1^2 \mathrm{Re})\}^{-1}$ and the global Reynolds number $\mathrm{Re} = u_\infty l_\infty \nu^{-1}$. Also, the predicted friction velocity $u_{\tau D}$ is given by

$$\frac{u_{\tau D}}{u_\infty} = a_1^{1/2}\varepsilon \tag{5.2}$$

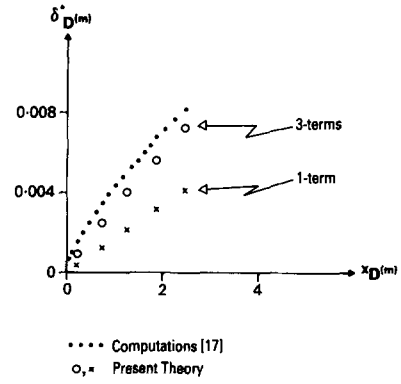

Fig. 3. Comparisons for the turbulent boundary-layer displacement: present work, (o, x); Cebeci et al.'s [17], computations, • • • .

to leading order. To start the comparisons we address Chevray and Kovasznay's [1] experiment for which Re $= 6.55 \times 10^5$, a value deduced from their Reynolds number $u_\infty \delta_\infty \nu^{-1}$ of 1.5×10^4 based on the "99% thickness" $\delta_\infty = 5.50\,\text{cm}$ at the trailing edge $x = 1$, $x_D = l_\infty = 240\,\text{cm}$. So here $\varepsilon = 0.103$, and then (5.1) predicts the ratio $\delta_D^*/l_\infty = 0.00299$ at the trailing edge $x = 1$, i.e., a displacement thickness $\delta_D^* = 0.72\,\text{cm}$ there. This compares not unfavourably with the value 0.84 cm deduced from Chevray and Kovasznay's findings and with the value 0.81 cm read from Cebeci et al.'s [17] computations (their Fig. 9), bearing in mind here and below the relative corrections omitted in the formulae such as (5.1), (5.2). Extending the comparisons of δ_D^* to other x values, we obtain the results shown in Fig. 3: see also Fig. 4(b) below. The agreement between (5.1) and the experiments or full computations is qualitatively very good throughout and quantitatively it seems to be fairly encouraging, for example being to within about 11% at the trailing edge. Near the leading edge the increased displacement slope $\propto -\varepsilon^3 \ln x$ implied by (5.1) appears to mirror well the increased slope observed in the full computations.

Again, the predicted value of $u_{\tau D}/u_\infty$ from (5.2) is 0.0412 for the above experiment and this is reasonably close to the experimental values 0.046 and 0.037 quoted by Chevray and Kovasnay using, respectively, a Clauser plot and a wall-slope method. Notice incidentally that if we multiply our prediction for δ_D^* by 9/8, to line up the theory and the experiment exactly at the trailing edge, then the agreement in terms of δ_D^* is good for the entire boundary layer (see Fig. 3); such a 9/8 factor is also consistent with the ratio 0.046/0.0412 of the friction velocities mentioned above.

Similarly, the predicted momentum thickness θ of the boundary layer can be shown to be given by

$$\frac{\theta}{l_\infty} \equiv a_1 \int_0^\infty u(1-u)\,\mathrm{d}y = \frac{\delta_D^*}{l_\infty} - a_1 \varepsilon^3 \int_0^\infty u_1^2\,\mathrm{d}\bar{y} \tag{5.3}$$

to our order of working. So for the experiment discussed above the value $\theta = 0.65\,\text{cm}$ is obtained, compared with the experimental result of 0.58 cm. The agreement again is not unfavourable (and it is noteworthy that the ratio, 0.65/0.58, is again close to 9/8). The large wall-shear stress predicted from (3.9)–(3.10) also seems consistent with the velocity profiles at the trailing edge shown by Chevray and Kovasznay [1] and by Cebeci et al. [17].

Comparisons with the more recent experiments of Andreopoulos and Bradshaw [2] show a roughly similar degree of agreement. Their experiment has a plate length of 308 cm and a higher Reynolds number, Re $\approx 6.7 \times 10^6$, implying that $\varepsilon = 0.083$ and so our predicted values of δ_D^*, θ at the trailing edge are found to be 0.57 cm, 0.52 cm respectively, compared with their results 0.81 cm, 0.64 cm in turn (the latter reading is from their p. 643, although their Table 1 suggests the different value $\theta = 0.59$ cm). Further, they measure a skin-friction coefficient c_f of 0.0024, which is close to the theoretical value of $2a_1\varepsilon^2 = 0.0022$ derived from (3.10).

We turn now to comparisons of the *wake* properties. First, the predicted centre-line velocity of the wake has the form

$$u_{CL} \equiv \frac{(u_D)_{CL}}{u_\infty} = 1 + \varepsilon q_1(x), \tag{5.4}$$

to the present order of working, from (4.6), with $q_1(x)$ given graphically in Fig. 2. The comparison between (5.4) and the experimental and the computational results of [1], [17] is presented in Fig. 4(a) and is seen to be very close indeed, over the entire length of wake for which the experimental/computational results are available. A representative prediction, by the way, is for $x = 1.5$ say, i.e., $x_D = 360$ cm, where $q_1 \approx -2.08$ from Fig. 2, so that, with $\varepsilon = 0.103$ still, (5.4) gives $u_{CL} = 0.786$ which is very near the experimental/computational finding at 120 cm beyond the trailing edge.

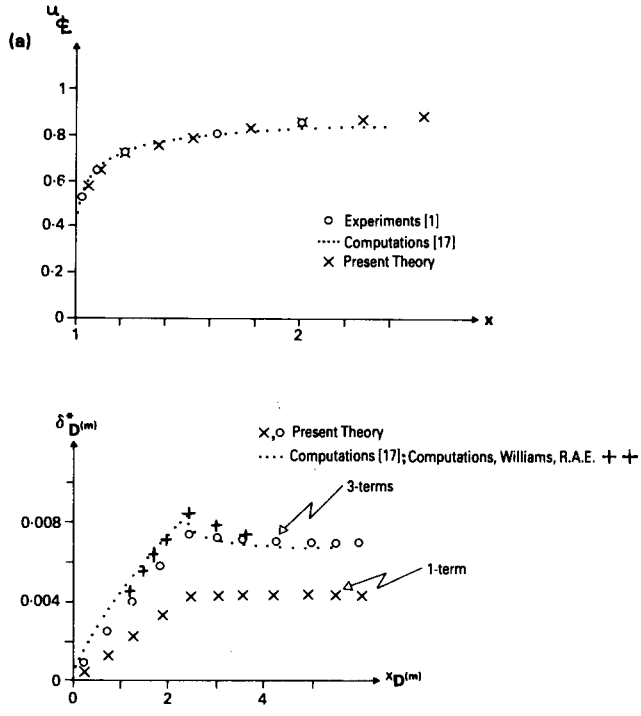

Fig. 4. Comparisons for the turbulent wake: (a) centre-line velocity, Re = 6.55×10^5 (x, present work) (o, Chevray and Kovasznay's [1] experiments) (· · · · , Cebeci et al.'s [17] calculations); (b) displacement thickness, Re = 6.55×10^5 (· · · · , computations [17]) (+ + +, computations by B.R. Williams, R.A.E., Farnborough, see text) (x, o, present theory); (c) centre-line velocity, Re = 6.7×10^6 (x, present work) (o, Andreopoulos and Bradshaw's [2] experiment).

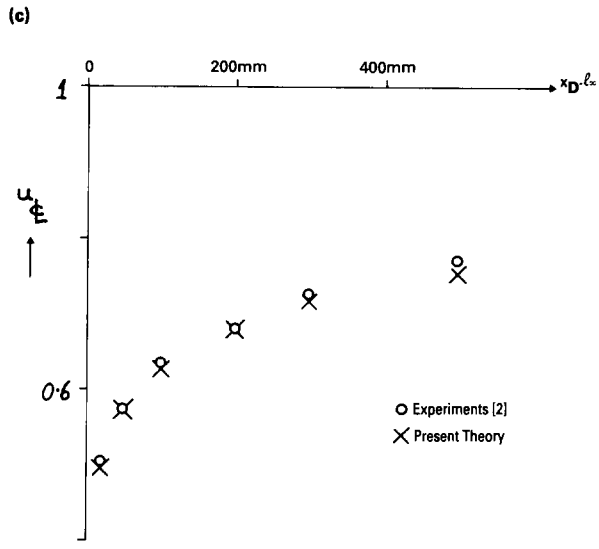

Fig. 4. Continued

Second here, the wake displacement thickness is predicted from Section 4 to be

$$\delta_D^* = l_\infty a_1[\varepsilon^2 - 4\varepsilon^3(\ln \varepsilon) + \varepsilon^3 \delta_2(x)] \tag{5.5}$$

where $\delta_2(x)$ is defined graphically in Fig. 2. The agreement (see Fig. 4(b)) with the experimental [1]/computational [17] results is very good qualitatively, with (5.5) giving a dip in displacement similar to, although less than, that observed just beyond the trailing edge (see also Appendix B) and reproducing the observed levelling out further downstream, and the agreement is also reasonably good overall in quantitative terms. Recent (1987) computations based on the R.A.E. lag-entrainment integral method, but coupled interactively with the outer flow, have kindly been done at R.A.E. Farnborough by B.R. Williams and supplied to us by S.P. Fiddes and these are also shown in Fig. 4(b), yielding a similar comparison.

The same level of agreement emerges from comparisons with Andreopoulos and Bradshaw's [2] experimental wake properties at a higher Reynolds number. In particular, the agreement concerning the wake centre-line velocity is very close, as shown in Fig. 4(c), while the trend of the wake displacement thickness in their results is the same as the theoretical one qualitatively and the quantitative agreement is again reasonable.

Further comparisons, of a more qualitative and structural nature, are included in the comments below.

6. Further discussion

The present theoretical findings for the symmetric turbulent wake flow are of direct interest, we believe, in three main respects. First, adopting the original Cebeci–Smith model throughout the wake as well as in the boundary layer does work (Section 4), producing solutions that satisfy the required symmetry conditions at the wake centre-line despite the presence of a cusp in the velocity profile slightly away from the centre line. Second, the resulting wake

solutions are physically sensible. Third, they show encouraging agreement with the experimental and fully computational findings* (Section 5), the comparisons being very close as regards the wake centre-line velocity and reasonably close in terms of the boundary-layer and wake displacement. This is especially so in view of the relative corrections in the theory: e.g., see Figs. 3, 4. An additional but smaller point here is that the computations of Cebeci et al. [17] for the flow past the flat plate address the TSL equations of Section 2 in the boundary layer, but in the wake their turbulence modelling is deliberately modified from the Cebeci–Smith form. The current work tends to suggest, therefore, that the modification in the wake is a very minor matter at the Reynolds numbers of interest and indeed it is almost certainly unnecessary.

The quantitative agreement on the boundary-layer and wake properties could be regarded as an added bonus, of course, since our original aim as in most asymptotic analysis was to gain some understanding of the structure of the high-Reynolds-number turbulent motion. The structure found appears to be in line with the experimental observations overall. Thus, concerning the wake in particular, the theory predicts an outer small-deficit layer of classical thickness $O(\varepsilon)$ (layer I in Section 3) but with an inner turbulent-laminar layer (layer III) of *non*-classical thickness $O(Re^{-2/3}\varepsilon^{-1/3})$, driven by the centre-line acceleration. This enhanced inner thickness, which is much larger than the classical wall-layer thickness of the oncoming turbulent boundary layer, seems to be present in Chevray and Kovasznay's [1] and Andreopoulos and Bradshaw's [2] experiments and in Cebeci et al.'s [3] calculations, for the velocity profiles, and in particular in Fig. 1 and Table 1 of [2]. The outer thickness, where initially the wake is little disturbed from its incident boundary-layer form, is also clearly noticable in the experiments of [1, 2] (e.g., see the comment on page 647, lines 4–5, of [2]), as is the predicted "cusp"-like behaviour of the wake velocity profile in the outer region: see [1]'s Fig. 1, [2]'s Fig. 3 and [3]'s Fig. 7. The corresponding centre-line velocity is nominally predicted as a small deficit from the freestream velocity for the majority of the wake, although the deficit increases logarithmically towards the trailing edge and is no longer a small deficit when the extra local zones around the trailing edge are entered: all these features agree also with the general experimental structure (see e.g., the comparisons in Section 5 and [2]'s empirical formula (1)). Associated with this, it is noteworthy that all the theoretical wake predictions turn out in fact to be rather general, in spite of our decision to adopt the Cebeci–Smith model throughout. The basic reason is that the "logarithmic layer" present in the incident boundary layer at the trailing edge is absent in almost all the wake and is replaced in effect by a "cuspidal layer" due to the necessary reduction in shear stresses near the centre line. Hence the detailed inner part $[1 - \exp(\ldots)]$ of the particular turbulence model taken in (2.6c) exerts no significant influence at all in the wake, the wake's inner layer being much thicker than $O(Re^{-1}u_\tau^{-1})$ as noted before; see also the end of the previous paragraph. So the only significant assumption in the turbulence model used for the wake is that the stress force B in (2.6b–d) is of the form $y^2|\partial u/\partial y|$ or (2.6d), predominantly, which is quite a general form.

The destruction of the initial logarithmic layer, incidentally, is achieved by a local lifting of the layer away from the centre line, very close to the trailing edge (Appendix B), with the layer finally petering out at the start of the near-wake (a) examined in Section 4.

---

* The present work agrees also with the recent Reynolds-averaged Navier-Stokes computations, based on the k–ε model, by V.C. Patel and H.C. Chen (Turbulent wake of a flat plate, *A.I.A.A. Jnl.* 25 (1987) 1078–1085), with regard to the main properties such as the wake centre-line velocity, the displacement thickness, the velocity profiles and so on, except in so far as the k–ε model underpredicts the far-wake growth, as the last-named authors mention. This paper was kindly pointed out to us by B.R. Williams and S.P. Fiddes.

On technical matters, further terms in the asymptotic analysis presented in Sections 3, 4 can be generated in principle and may well improve the agreement with the experiments, at least if the favourable effect of advancing from the one-term to the three-term prediction shown in Figs. 3, 4 is continued. Again, the further regions existing nearer the trailing edge, as discussed in Appendix B, are of interest not only theoretically but also physically. For one thing, many of the Andreopoulos and Bradshaw's [2] experimental measurements are taken quite close to the trailing edge, and, for another, it may be that the local trailing-edge analysis points the way towards the understanding of the turbulent-separation problem: see also below. A final technical point here concerns the solving of the boundary-layer and wake equations in (3.3a)ff.. A helpful approximation to, and check on, the solution can be derived from neglecting the outer part $y > y_1$ of the boundary layer or wake, based on the supposition that a_5 in (2.6d) is sufficiently small (≈ 0.1). With that approximation the upper constraint on the O(ε) layer I becomes $u_1 = \partial u_1/\partial \bar{y} = 0$ at the unknown upper boundary $\bar{y} = \bar{y}_1(x)$ and then only the inner part (2.6c) of the turbulence model plays a role. In the boundary layer, for instance, the approximation leads to the values 2, $1 - \ln 2 (= 0.307)$ and zero for η_1, b_1, c_1, in turn, instead of the values listed in (3.16c), while the integral in (3.17) becomes 5/3 as opposed to the value 1.68 noted before. Similar, fairly close, estimates result from using this approximation in the far-wake as well, and it may prove useful in other contexts.

Work by the authors is in progress to apply/extend the present theoretical approach to more realistic airfoils and conditions. First, the flows past many thicker but not too thick airfoils fall fairly readily into the present category of attached turbulent motions, we believe, and application of the structural theory seems called for there. Second, the interactive-boundary-layer treatments that have been applied to turbulent flows with the possibility of separation occurring can be investigated along similar lines: see also Appendix B. Third, for bluff airfoils, including the circular cylinder, the question of the structure of turbulent separation needs further study. At present our work in progress tends to indicate that only small-scale, not large-scale, separation can occur at high Reynolds numbers in such cases. If so, this emphasizes the value of analyses of classical turbulent boundary layers, such as in the current work, which among other things explains how a logarithmic layer can be lifted away from a surface (see an earlier paragraph) and then peters out, a phenomenon commonly associated also with separation. Fourth, compressibility effects need to be incorporated in the theory in order to tackle the interaction and possible separation, be it local or large-scale, occurring between an incident shock wave and a turbulent boundary layer. A suggestion from this work relevant to all the above, we feel, is that the use of a particular turbulence model, here the Cebeci–Smith one, can lead to physically realistic and accurate predictions when a turbulent boundary layer encounters a significant change in boundary conditions.

Acknowledgement

Helpful discussions with S.P. Fiddes, M.C.P. Firmin, R.E. Melnik and J.H.B. Smith are gratefully acknowledged, as are a referee's comments and the financial support for A.N. from the Department of Trade and Industry, U.K., through R.A.E. Farnborough.

Appendix A. Alternative derivations of the boundary-layer and wake properties

This is to record briefly two alternative approaches for deriving the turbulent boundary-layer and wake features.

First, the normalization in (2.5) was applied earlier for convencience. Instead we could simply deal with $(u_D, v_D)/u_\infty$, $(x_D, y_D)/l_\infty$, i.e., replace the factor a_1 in (2.5) by unity so that an a_1 factor is inserted in (2.6) and Re replaces R there, and then expand for large Re, analogous to (3.2). The analysis proceeds much as in the main text and yields, for example,

$$\frac{\delta_D^*}{l_\infty} = \varepsilon_1^2 a_1 x + \varepsilon_1^3 \ln(\varepsilon_1)(-4a_1 x) + a_1 \varepsilon_1^3 \{(-1.74)x - 2x \ln(x a_1^3)\} \tag{A1}$$

in the boundary layer, with $\varepsilon_1 \equiv 1/\ln \mathrm{Re}$. The result (A1) is the same to $O(\varepsilon^3)$ as the prediction in Section 3 and numerically it gives values close to those presented in Section 5. A similar correspondence holds in the wake analysis.

Second, suppose we refer instead to the corresponding Navier–Stokes equations with the same turbulence model, thus seeking a more complete account than from the TSL equations (2.6). At large Reynolds numbers the only difference encountered, to our order of working, comes from the external induced pressure which is typically $O(\varepsilon^2)$ due to the external potential flow past the displacement surface of typical slope $O(\varepsilon^2)$, from δ_1. Hence the third-order problem quoted in (3.6) remains intact except for the outer boundary condition which becomes

$$u_2 \to -p_2(x) \quad \text{as} \quad \bar{y} \to \infty \tag{A2}$$

where $\varepsilon^2 p_2$ is the induced pressure p, given by

$$p_2(x) = -\frac{1}{\pi} \int_0^\infty \frac{\delta_1'(\xi)\, \mathrm{d}\xi}{x - \xi}. \tag{A3}$$

The alteration has no effect on the predictions in the main text, to the orders shown, i.e. to $O(\varepsilon)$ in u_{CL} and $O(\varepsilon^3)$ in δ_D^*/l_∞. For

$$\delta_2 = -\int_0^\infty (u_2 + p_2(x))\, \mathrm{d}\bar{y} \tag{A4}$$

now, so that on integration across the flow the results (3.14) and (4.7) for $\delta_2(x)$ still hold. Again, the solution here is closely related to the TSL one anyway, with

$$[u_1, u_{2L}, u_2] \text{ (Navier–Stokes)} = [u_1, u_{2L}, u_2 + p_2] \text{ (TSL)} \tag{A5}$$

in schematic form. Significant differences arise only at higher order as regards the main text, therefore, although a more substantial effect can be seen in Appendix B below.

Appendix B. Trailing-edge zones

Concerning the TSL version (2.6) first, the nonuniformities in the near wake of Section 4(a) are smoothed out by a single localized trailing-edge zone of small length scale $O(R^{-1}\varepsilon^{-1})$: see Fig. 5. Approximately, the near wake exhibits two thinning layers emerging as $x \to 1+$, one of width $O[\varepsilon(x-1)]$ from (4.9) and the other of width $O[R^{-2/3}\varepsilon^{-1/3}(x-1)^{1/3}]$ since, in the governing equation (4.4a) for the inner sublayer III, $q_1' \sim (x-1)^{-1}$ as $x \to 1+$. The two layers appear to become coincident when $x - 1 \sim R^{-1}\varepsilon^{-2}$, therefore; this estimate for the new local zone is affected by logarithmic matching terms however and we find instead the main length scale $O(R^{-1}\varepsilon^{-1})$, subject to the matching described later in the Appendix. An estimate based on velocity scales agrees with the above. With $x = 1 + R^{-1}\varepsilon^{-1}\tilde{x}$ and $y = R^{-1}\varepsilon^{-1}\tilde{y}$, then, the local zone has

$$(u, v) = \varepsilon(\bar{\bar{u}}, \bar{\bar{v}})(\tilde{x}, \tilde{y}) + \cdots \tag{B1}$$

and so from (2.6) the governing equations and boundary conditions are

$$\frac{\partial \bar{\bar{u}}}{\partial \tilde{x}} + \frac{\partial \bar{\bar{v}}}{\partial \tilde{y}} = 0, \tag{B2}$$

$$\bar{\bar{u}}\frac{\partial \bar{\bar{u}}}{\partial \tilde{x}} + \bar{\bar{v}}\frac{\partial \bar{\bar{u}}}{\partial \tilde{y}} = \frac{\partial}{\partial \tilde{y}}\left[\tilde{y}^2\{1 - \exp(-a_6\tilde{y})\}^2\left(\frac{\partial \bar{\bar{u}}}{\partial \tilde{y}}\right)^2\right] + \frac{\partial^2 \bar{\bar{u}}}{\partial \tilde{y}^2}, \tag{B3}$$

$$\bar{\bar{u}} = \bar{\bar{v}} = 0 \quad \text{at} \quad \tilde{y} = 0, \ \tilde{x} < 0, \tag{B4}$$

$$\partial \bar{\bar{u}}/\partial \tilde{y} = \bar{\bar{v}} = 0 \quad \text{at} \quad \tilde{y} = 0, \ \tilde{x} > 0, \tag{B5}$$

$$\bar{\bar{u}} \to \tilde{u}(\tilde{y}) \quad \text{as} \quad \tilde{x} \to -\infty, \tag{B6}$$

$$\bar{\bar{u}} \sim \ln(\tilde{y}) \quad \text{as} \quad \tilde{y} \to \infty. \tag{B7}$$

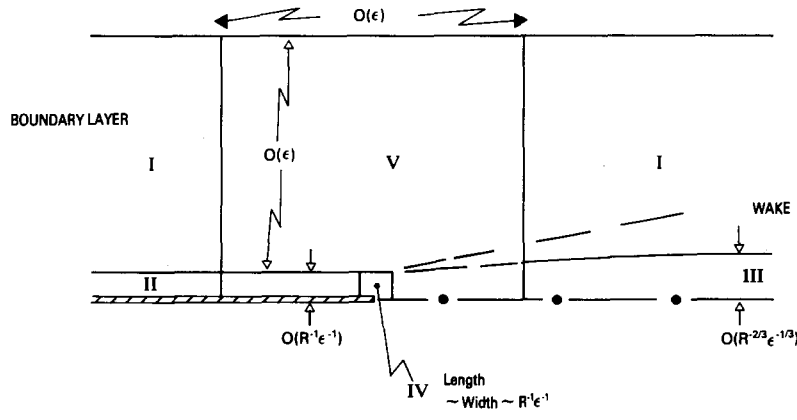

Fig. 5. The flow structure surrounding the trailing edge according to Appendix B. The O(ε) by O(ε) region V is inactive in the TSL version.

Here (B4), (B5) are constraints representing trailing-edge conditions, while (B6), (B7) join with layer II upstream and with the majority of the boundary-layer-to-wake flow outside where $\bar{y}$ is O(1). There the solution is more regular, with

$$u = 1 + \varepsilon f_1(\bar{y}) + \varepsilon^2 \ln \varepsilon u_{2L}(1, \bar{y}) + O(\varepsilon^2) \tag{B8}$$

for $x - 1 = \varepsilon\tilde{x}$ of order ε, where the functions shown are those defined in Section 3, thus yielding the logarithmic constraint in (B7). The local problem posed by (B2)–(B7) is nonlinear, consisting of virtually the whole system (2.6), and in general it requires a numerical treatment, except that the solution for $\tilde{x} < 0$ is identically $\bar{\tilde{u}} = \tilde{u}(\tilde{y})$ since there is no upstream influence here. For small positive $\tilde{x}$ a Goldstein-like $O(\tilde{x}^{1/3})$ sublayer is present, as in laminar flow. For large positive $\tilde{x}$ the match far downstream with Section 4(a) can be verified. There the local flow of (B2)–(B7) splits into two parts. The outer part has $\tilde{y}$ increasing almost linearly with $\tilde{x}$; in fact $\tilde{y} = \tilde{x}(\ln \tilde{x})^{-1}\xi_1$ and

$$\bar{\tilde{u}} \sim \ln \tilde{x} - \ln (\ln \tilde{x}) + G_1(\xi_1) \tag{B9}$$

where from substitution into (B2)–(B7) G_1 satisfies

$$1 - \xi_1 G_1' = (\xi_1^2 G_1'^2)'. \tag{B10}$$

This is exactly the equation (4.9b) and so yields the cuspidal behaviour as $\xi_1 \to 0+$. The necessary inner part therefore has $\tilde{y}$ smaller but still large, $\tilde{y} = \tilde{x}^{1/3}(\ln \tilde{x})^{-1/3}\xi_2$ and

$$\bar{\tilde{u}} \sim \ln \tilde{x} + \cdots + \tilde{x}^{-1/3}(\ln \tilde{x})^{1/3} G_2(\xi_2). \tag{B11}$$

So G_2 is governed by

$$1 = (\xi_2^2 G_2'^2)' + G_2'', \tag{B12}$$

which is the same as (4.4a), in its similarity form as $x \to 1+$, allowing the solution (4.4b–d). Thus we have the beginnings of the "cusp" layer taking over from the upstream "logarithmic" layer. The outer part where ξ_1 is O(1) matches with the near-wake structure of Section 4(a) since the outer part's width $\sim R^{-1}\varepsilon^{-1}\tilde{x}(\ln \tilde{x})^{-1}$ becomes of order $\varepsilon(x - 1)$ downstream when $\tilde{x} \to R\varepsilon(x - 1)$. Likewise, the inner part merges into the thickened sublayer III of Section 4.

A not dissimilar local interactive process occurs on the basis of the turbulent Navier–Stokes equations also: see Appendix A. Thus the innermost zone is given by (B1) again but with (B3) then being replaced by the full Navier–Stokes equations, subject to (B4)–(B7) again and, in view of the ellipticity present here, to the matching requirements (B9)–(B12). It can be verified that (B9)–(B12), which were derived above from the TSL equations, emerge also from a downstream analysis of the Navier–Stokes equations, thus providing the join with Section 4(a). The local solution is now no longer trivial in $\tilde{x} < 0$, but for $\tilde{x}$ small and positive an $O(\tilde{x}^{1/3})$ sublayer is almost certainly involved again although it is more of the Rott–Hakkinen kind than the Goldstein kind mentioned above. Lastly, the majority of the boundary-layer-to-wake motion outside again has the form in (B8) but with the $O(\varepsilon^2)$ term

being controlled by equations different from the TSL version because the x- and y- dependences are comparable and the induced pressure variation is $O(\varepsilon^2)$, from Appendix A. The above local structure seems to correct that in [15] and connects with other work [9, 16] on trailing edge zones, and in addition it can be extended to different trailing-edge geometries as described in our subsequent work [24].

Appendix C. Numerical solution of the wake problem

The predictor–corrector method used for the wake problem defined in Section 4 is as follows. First, in view of the cuspidal behaviour implied in (4.2b) the transformation $\bar{y} = z^2$ is applied, so that (3.3b) becomes

$$\frac{\partial u_1}{\partial x} = \begin{cases} \dfrac{1}{8z}\dfrac{\partial}{\partial z}\left[z^2\left(\dfrac{\partial u_1}{\partial z}\right)^2\right], & z < \hat{z}, \\ \dfrac{a_5}{4z}\dfrac{\partial}{\partial z}\left(z^{-1}\dfrac{\partial u_1}{\partial z}\right), & z > \hat{z}, \end{cases} \tag{C1}$$

with the result $\delta_1 = 1$ inserted. Given the solution $u_1 = \bar{u}_1$, say, at any station x, the predictor stage for the next station $(x + \Delta x)$ takes the form

$$u_{1j}^{(p)} = \bar{u}_{1j} + \Delta x M(\bar{u}_{1j}) \tag{C2}$$

for $2 \leqslant j \leqslant K - 1$. Here the discretization in z has $z = z_j = (j - 1)\Delta z$, with $1 \leqslant j \leqslant K$, and

$$M(u_j) = \begin{cases} \dfrac{(u_{j+1} - u_{j-1})}{8\Delta z}\left\{\left(\dfrac{u_{j+1} - u_{j-1}}{2\Delta z}\right) + z_j\dfrac{(u_{j+1} - 2u_j + u_{j-1})}{(\Delta z)^2}\right\} & \text{for } z < \hat{z}, \\ \dfrac{a_5}{4z_j}\left\{-\left(\dfrac{u_{j+1} - u_{j-1}}{2z_j^2\Delta z}\right) + \dfrac{(u_{j+1} - 2u_j + u_{j-1})}{z_j(\Delta z)^2}\right\}, & \text{for } z > \hat{z}. \end{cases}$$

The centre-line and the outer values u_{11}, u_{1K} are then determined by $u_{1K}^{(p)} = 0$ and

$$u_{11}^{(p)} = \bar{u}_{11} + \frac{\Delta x}{4}\left(\frac{\bar{u}_{12} - \bar{u}_{11}}{\Delta z}\right)^2, \tag{C4}$$

the latter being the finite-difference version of (4.2b) in effect. The corrector stage then takes

$$u_{1j}^{(c)} = \left(\frac{u_{1j}^{(p)} + \bar{u}_{1j}}{2}\right) + \frac{\Delta x}{2}M(u_{1j}^{(p)}) \tag{C5}$$

for $2 \leqslant j \leqslant K - 1$, with $u_{1K}^{(c)} = 0$ and

$$u_{11}^{(c)} = \left(\frac{u_{11}^{(p)} + \bar{u}_{11}}{2}\right) + \frac{\Delta x}{8}\left(\frac{u_{12}^{(p)} - u_{11}^{(p)}}{\Delta z}\right)^2 \tag{C6}$$

analogous to (C4). The above allows the wake calculation to be marched forward in small steps Δx from the trailing edge at $x = 1$ and the integral for the displacement contribution δ_2 is evaluated from the trapezium rule at each step. The junction $z = \hat{z}(x)$ in (C1), (C3) is fixed by the test

$$z_j^3 \left(\frac{\bar{u}_{1j+1} - \bar{u}_{1j-1}}{2\Delta z} \right) \gtrless 2a_5, \tag{C7}$$

applying for $z \lesseqgtr \hat{z}$.

A special treatment is needed at the very first step, however, because of the logarithmic singularity in (4.5) at $\bar{y} = 0$. A satisfactory procedure for handling this was found, after some trials, to be simply to replace the $\ln(\bar{y})$ term, implied in (4.5), by $\ln(\bar{y} + h)$ with h a small positive constant, the rest of the solution at $x = 0$ being given by (3.16). Numerical solutions were then generated in $x > 1$ for various small values of h (10^{-2} to 10^{-6}) and the required solution was derived by extrapolation of the results. In practice the value $h = 10^{-6}$ turned out to be sufficiently small for graphical accuracy, for instance.

This simple scheme is second-order accurate overall, as grid-size studies bear out, and it proved stable for sufficiently small steps Δx. Typical values taken for Δx, Δz, K were 10^{-3}, 0.05, 201 respectively and Fig. 6 summarizes the effects of varying the grid size, as well as the parameter h. Extrapolation from these results was used to obtain the results shown previously in Figs. 2, 4.

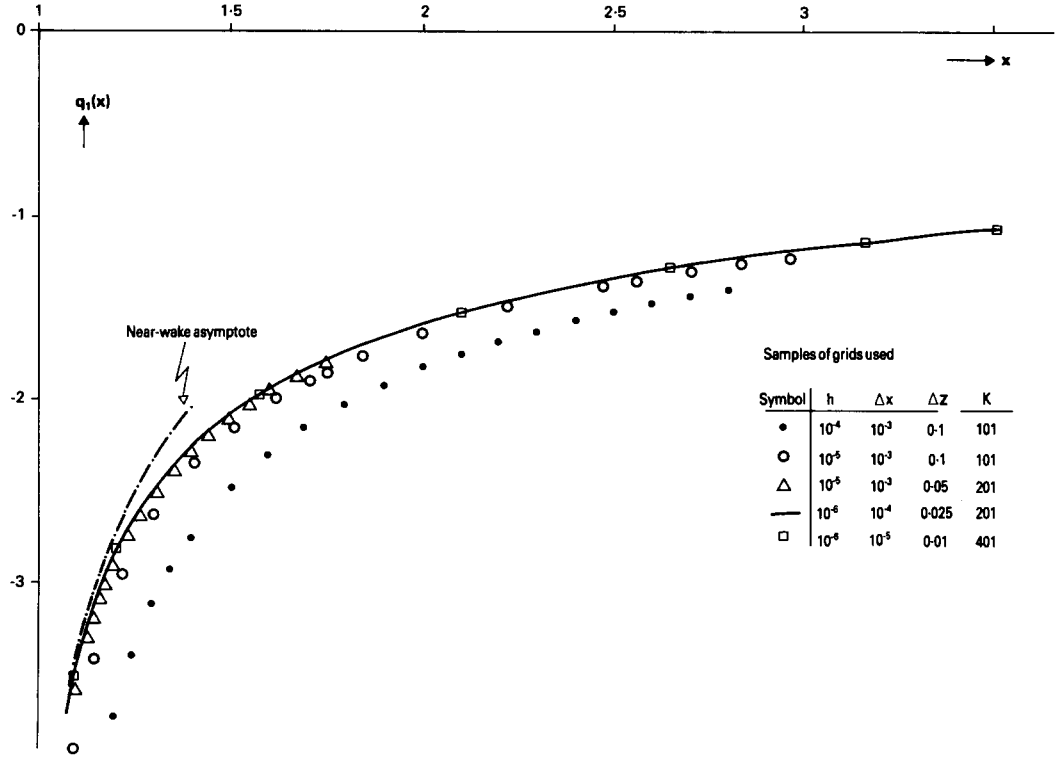

Fig. 6. Further details of the present work's computations for the wake flow: see Appendix C. The values of [h, Δx, Δz, K] used in the computations are as shown.

References

1. R. Chevray and L.S.G. Kovasznay, Turbulence measurements in the wake of a thin flat plate, *A.I.A.A. Jnl.* 7 (1969) 1641–1643.
2. J. Andreopoulos and P. Bradshaw, Measurements of interacting turbulent shear layers in the near wake of a flat plate, *J. Fluid Mech.* 100 (1980) 639–668.
3. P.J. Pot, Measurements in a 2D wake and in a 2D wake merging into a boundary layer, Nat. Aerosp. Lab. report no. NLR TR 79063 U, The Netherlands (1979).
4. B.R. Ramaprian, V.C. Patel and M.S. Sastry, The symmetric turbulent wake of a flat plate, *A.I.A.A. Jnl.* 20 (1982) 1228–1235.
5. G.L. Mellor, The large Reynolds number, asymptotic theory of turbulent boundary layers, *Int. J. Eng. Sci.* 10 (1972) 851–873.
6. W.B. Bush and F.E. Fendell, Asymptotic analysis of turbulent channel and boundary-layer flow, *J. Fluid Mech.* 56 (1972) 657–668.
7. F.E. Fendell, Singular perturbation and turbulent shear flow near walls, *J. Astro. Sci.* 20 (1972) 129–165.
8. R.E., Melnik, R. Chow and H.R. Mead, Theory of viscous transonic flow over airfoils at high Reynolds numbers, A.I.A.A., paper no. 77–680 (1977), presented at 10th. Fluid and Plasma Dyn. Conf., Albuquerque, NM, USA, June 27–29.
9. R.E. Melnik and B. Grossman, On the turbulent viscid-inviscid interaction at a wedge-shaped trailing edge, Proc. 1st Symp. Num. and Phys. Aspects of Aerod. Flows, Long Beach, CA, USA (ed. T. Cebeci), Springer-Verlag (1982).
10. R.E. Melnik, Turbulent interactions on airfoils at transonic speeds – recent developments, paper no. 10, N.A.T.O. AGARD Symp. Comput. of Viscous–Inviscid Flows, Colorado Springs, CO, USA, Sept. 29–Oct. 1 (1980).
11. R.E. Melnik, A new asymptotic theory of turbulent boundary layers and the turbulent Goldstein problem, Proc. IUTAM Symp. Boundary-Layer Separation, (eds. F.T. Smith and S.N. Brown), Springer–Verlag (1987).
12. R.I. Sykes, An asymptotic theory of incompressible turbulent boundary-layer flow over a small hump, *J. Fluid Mech.* 101 (1980) 647–670.
13. V. V. Sychev and Vik. V. Sychev, On turbulent separation, *Zh. Vyssh. Mat. Mekh. Fiz.* 20 (1980) 1500–1512.
14. V. V. Sychev, On turbulent boundary layer separation, Proc. IUTAM Symp. Boundary-Layer Separation, (eds. F.T. Smith and S.N. Brown), Springer–Verlag (1987).
15. I.E. Alber, The turbulent wake of a thin flat plate, *A.I.A.A. Jnl.* 18 (1980) 1044–1051.
16. E.A. Bogucz and J.D.A. Walker, Analysis and prediction of the turbulent near wake at a sharp trailing edge (1987), to be submitted to *J. Fluid Mech.*.
17. T. Cebeci, F. Thiele, P.G. Williams and K. Stewartson, On the calculation of symmetric wakes, I: Two-dimensional flows, *Num. Heat Trans.* 2 (1979) 35–60.
18. T. Cebeci and A.M.O. Smith, *Analysis of turbulent boundary layers*, Academic Press, New York (1974).
19. M. Inouye, S.G. Marvin and Y.S. Sheaffer, Turbulent-wake calculations with an eddy viscosity model, *A.I.A.A. Jnl.* 10 (1972) 216–217.
20. T. Cebeci, K. Stewartson and J.H. Whitelaw, Calculation of two-dimensional flow past airfoils, Proc. 2nd Symp. Num. and Phys. Aspects of Aerod. Flows, ed. T. Cebeci, Springer–Verlag (1984).
21. P. Bradshaw, Prediction of the turbulent near-wake of a symmetrical airfoil, *A.I.A.A. Jnl.* 8 (1970) 1507–1508.
22. G.D. Hoffman and B.S.H. Ny, Modelling of an asymmetric turbulent near wake using the interaction hypothesis, *A.I.A.A. Jnl.* 16 (1978) 193.
23. A.C. Trupp, R.S. Azad and S.Z. Kassab, in: *Experiments in Fluids*, Springer–Verlag (1986).
24. A. Neish and F.T. Smith, (1987), in preparation.
25. A. Neish, Ph.D. Thesis, Univ. of London (1987), in preparation.
26. A.F. Messiter, Boundary layer flow near the trailing edge of a flat plate, *SIAM J. Appl. Math.* 18 (1970) 241–257.
27. K. Stewartson, On the flow near the trailing edge of a flat plate – II, *Mathematika* 16 (1969) 106–121.
28. A.F. Messiter, Boundary-layer interaction theory, *Trans. A.S.M.E., J. Appl. Mech.* 50 (1983) 1104–1113.
29. F.T. Smith, Steady and unsteady boundary-layer separation, *Ann. Rev. Fluid Mech.* 18 (1986) 197–220.